TM-71-2015-2

TECHNICAL MEMORANDUM

THE LUNAR MICROMETEOROID EXPERIMENT, L033

Bellcomm

BELLCOMM, INC.
955 L'ENFANT PLAZA NORTH, S.W., WASHINGTON, D.C. 20024

COVER SHEET FOR TECHNICAL MEMORANDUM

TITLE- The Lunar Micrometeoroid Experiment, L033

TM- 71-2015-2

FILING CASE NO(S)- 340

DATE- April 20, 1971

AUTHOR(S)- J. S. Dohnanyi

FILING SUBJECT(S) (ASSIGNED BY AUTHOR(S))- Micrometeoroid Experiment

ABSTRACT

Use of the Pioneer 7 and 8 cosmic dust detectors in the Lunar Ejecta and Micrometeorites (LEAM) experiment of O. E. Berg and coinvestigators is discussed. All sensors of the LEAM experiment should record secondaries at rates that exceed the detection rate of primaries by one or two orders of magnitude. This follows from the sensitivity of the sensors to the energy and momentum distribution of primary micrometeoroids and secondary lunar ejecta, as well as to the angular distribution of ejecta. The great majority of secondaries will impact the sensors on the descending portion of their trajectories. The contribution of meteor showers is expected to be small. These general conclusions follow from a LEAM performance analysis that is based on a model for the distribution of secondary ejecta and on estimates of primary and secondary impact rates. Subject to revision that may be necessary after precise calibration of the sensors, the present results provide a method for deriving the mass, velocity and angular distribution from experimental impact data, once these become available.

DISTRIBUTION

COMPLETE MEMORANDUM TO

CORRESPONDENCE FILES:

OFFICIAL FILE COPY
plus one white copy for each additional case referenced

TECHNICAL LIBRARY (4)

NASA Headquarters
R. J. Allenby - MAL
C. T. D'Auitolo - RV-1
D. A. Beattie - MAL
M. Dubin - SG
A. S. Lyman - MR
W. T. O'Bryant - MAL
R. A. Petrone - MA
L. R. Scherer - MAL
NASA Hq. Library - USS-10

Manned Spacecraft Center
P. B. Burbank - TG
A. J. Calio - TA
B. G. Cour-Palais - TG2
P. W. Gast - TN
T. Guili - TG
D. Kessler - TG2
M. G. Simmons - TA
H. A. Zook - TG2

Manned Space Flight Center
K. S. Clifton - R-SSL-PM
C. C. Dalton - R-AERO-Y
R. J. Naumann - R-SSL-PM

Goddard Space Flight Center
O. E. Berg - 613
R. G. Roosen - 614

Langley Research Center
J. M. Alvarez - AMPD
J. R. Davidson - SRD
D. D. Davis, Jr. - AMPD
C. A. Gurtler - FID
W. H. Kinard - AMP

Ames Research Center
H. J. Allen - D
B. S. Baldwin, Jr. - STT

COMPLETE MEMORANDUM TO

Ames Research Center (Cont'd.)
N. H. Farlow - SSP
D. E. Gault - SSP
J. F. Kerridge - Planetary Branch
C. R. Nysmith - SCHI
J. L. Summers - SVHI

Jet Propulsion Laboratory
A. Bratenahl
A. F. H. Goetz
J. D. Jaffe

ITT Research
W. K. Hartmann

Cornell University
Carl Sagan

University of California
H. Alfven
G. Arhenius

Baylor University
W. M. Alexander

Douglas Aircraft
J. K. Wall

Department of Interior
S. F. Singer

Dudley Observatory
C. Hemenway

John Hopkins University
Department of Geology
A. H. Marcus

Ohio State University
Physics Department
J. Korringa

Rice University
J. J. W. Rogers

Smithsonian Astrophysical Observatory
A. F. Cook

DISTRIBUTION LIST (CONT'D.)

Complete Memorandum to

Smithsonian Astrophysical Observatory
E. L. Fireman
L. Jacchia
B. G. Marsden
R. E. McCrosky
Z. Sekanina
R. B. Southworth
F. L. Whipple
F. W. Wright

TRW
J. Friichtenicht

University of California Inst. of Geophyiscs and Planetary Physics
E. Anders

University of Arizona
Lunar & Planetary Laboratory
T. Gehrels

Valley Forge Space Technology Center
R. Soberman

Bellcomm, Inc.
A. P. Boysen, Jr.
J. O. Cappellari, Jr.
F. El-Baz
D. R. Hagner
W. G. Heffron
J. J. Hibbert
N. W. Hinners
M. Liwshitz
K. E. Martersteck
J. Z. Menard
G. T. Orrok
J. W. Timko
R. L. Wagner
All Members Department 2015
Central Files
Department 1024 Files
Library

Abstract Only to

Bellcomm, Inc.
D. A. Bass
J. P. Downs
T. B. Hoekstra
D. P. Ling
J. L. Marshall
P. E. Reynolds
P. F. Sennewald
R. V. Sperry
A. W. Starkey
A. R. Vernon
M. P. Wilson
D. B. Wood

BELLCOMM, INC.
955 L'ENFANT PLAZA NORTH, S.W. WASHINGTON, D. C. 20024

SUBJECT: The Lunar Micrometeoroid Experiment, LO33 - Case 340

DATE: April 20, 1971

FROM: J. S. Dohnanyi

TM-71-2015-2

TECHNICAL MEMORANDUM

1. Introduction

The "Lunar Ejecta and Meteorites" experiment, by O. E. Berg and co-investigators (D. E. Gault and N. Farlow) is scheduled to fly on the Apollo 17 mission. The purpose of the experiment is to measure the primary and secondary meteoroid fluxes on the lunar surface as a function of time and incoming direction of the particles. This would yield information on the spatial and temporal distribution of primary particles and the corresponding flux density of secondaries. In order to gain further insight about the information this experiment is likely to provide, we undertook a review of the performance characteristics of the instrument and the environment to be measured. The result is a quantitative estimate of the data that will be obtained and of their physical significance.

2. The Experiment

The experiment is similar to those successfully flown on the Pioneer 8 and 9 satellites (Berg and Richardson, 1969). It consists of several particle detectors, each one arranged to intercept the meteoroid flux in a different direction. Each detector consists of two parallel detecting surfaces 5 cm apart: an outer surface A and a rear surface B. The two surfaces detect the impact ionization produced during an event while a microphone, mounted behind the B surface, detects momentum.

Impact ionization at surfaces A and B is detected by means of a film-grid-array, schematically shown in Figure 1. It can be seen, in Figure 1, that both the A and B surfaces consist of four film strips positioned between transverse grid strips, as indicated. A measurement is obtained when a hypervelocity particle impacts the sensor with sufficient energy to produce measurable impact ionization at A; because of the 24 volt bias in the film-grid-system, positive ions will be collected at the film of A and electrons at the grid of A. If the particle has enough energy, it will proceed and impact the film of B and again

produce detectable impact ionization. Each film and each grid is separately instrumented so that the particular A and B film and grid strips which register an event are automatically identified, the film signals are pulse-height analyzed and the time lapse between the impact on A and subsequent impact on B is read out (if B is impacted). The sensor can therefore be regarded as an arrangement of two parallel "chess boards" where impacts into any particular square are identified; if a particle has sufficient energy to register at both A and B surfaces, then its time of flight as well as direction of flight is recorded, permitting a calculation of its orbit.

Tests with the electrostatic particle accelerator at GSFC indicate a proportionality between particle energy and impact ionization for iron projectiles. Detectable ionization is observed for projectiles having a threshold velocity of about 1.5 km/sec or greater.

Current plans for the lunar surface experiment include a deployment of 3 sensors, forming faces of a prism. Each sensor will have an area of 100 cm^2. One sensor is in the horizontal plane, "looking" up. Two sensors are in the vertical plane, one looking east and the other west; their geometrical center is about 26 cm above ground. The horizontal sensor and the east looking one are complete with A and B films 5 cm apart, and are capable of performing time of flight measurements. The west looking sensor is equipped with B-film and grid only and with two microphones. These microphones have a collecting area of 1" x 4" and 3" x 4". In addition, there are microphones on the horizontal and the east looking sensor, each with a collecting area of 4" x 4".

The microphones are each designed to detect particles having a momentum in excess of 2×10^{-5} dyne-sec. The A-film grid system is designed to detect particles having kinetic energies in excess of .2 ergs and a velocity in excess of 1.5 km/sec; the B-film detects particles with energies in excess of .1 ergs and velocities higher than 1.5 km/sec.

3. Flux Model

For the flux $f(m)dm$ of primary sporadic meteoroids in a mass range m to m+dm per square meters per second per 2π steradian incident into earth's atmosphere, we take (Dohnanyi, 1970).

$$f(m)dm = Am^{-\alpha}dm, \quad m \geq \mu \tag{3.1}$$

$$= A\mu^{-\alpha+\beta}m^{-\beta}dm, \quad m \leq \mu \tag{3.2}$$

where

$$A = 3 \times 10^{-18} (Kg)^{\alpha-1}, \quad \alpha = 13/6, \quad \beta = 3/2. \tag{3.3}$$

The quantity μ is the meteroid mass at which, on a doubly logarithmic plot, the plot of f(m) changes from a flatter slope for $m \leq \mu$ to a steeper one for $m \geq \mu$.

In order to estimate μ, we use recent data by Berg and Gerloff (1970) and Gerloff and Berg (1970). These authors found that the cumulative flux N(m), measured by the Pioneer 8 and 9 cosmic dust detectors, of particles having a mass m* or greater is:

$$N(m^*) = 2 \times 10^{-4} \text{ particles/m}^2 \text{ sec } 2\pi \text{ sterad} \tag{3.4}$$

where

$$m^* = 5 \times 10^{-15} Kg. \tag{3.5}$$

For masses smaller than m* a cutoff in the population of micrometeoroids is indicated. In order to use Eq. 3.4 to define μ in Eq. 3.1 we note that fluxes measured by the Pioneer probes are deep space fluxes. The gravitational field of the earth increases its meteoroid capture cross section and hence the near earth meteoroid flux as has been discussed by Opik (1951).

It can be shown that (Dohnanyi, 1966)

$$f_{m,v}(1)\,dmdv = f_{m,v}(E)\,dm\,dv\,[1+v_e^2\,(E^{-1}-1)/(v^2+v_e^2)]^{-1} \tag{3.6}$$

where $f_{m,v}(E)\,dmdv$ is the flux of meteoroids per square meter sec 2π sterad in the mass range m to dm having a geocentric velocity in the range of v to v+dv at a distance E from the center of the earth, E is in units of earth radii, and v_e is the escape velocity; thus E=1 refers to the earth's surface and $E = \infty$ refers to deep space.

Averaging Eq. 3.6 over the eight velocity determinations provided by the Pioneer data (Berg and Gerloff, 1970 and Gerloff and Berg, 1970) one obtains

$$f_m(1)\,dm = 1.9\ f_m(\infty)\ dm. \tag{3.7}$$

This focussing factor of 1.9 compares favorably with the value of 1.8 obtained for photographic meteors (Dohnanyi, 1966).

We now let

$$\int_{m^*}^{\infty} f(m)\,dm = 1.9N(m^*) \qquad (3.8)$$

where f(m) is given by Eq's 3.1, 3.2, and 3.3 and the right hand side of Eq. 3.7 is given by Eq. 3.4 and 3.5. Solving Equation 3.8 for μ, we get

$$\mu = 1.14 \times 10^{-10}\ \text{Kg}. \qquad (3.9)$$

In view of existing uncertainties Eq. 3.9 is readily approximated by

$$\mu = 10^{-10}\ \text{Kg} \qquad (3.10)$$

which is the value we shall adopt in this paper. This defines the model flux near earth.

In order to estimate the meteoroid flux on the lunar surface, we have to calculate the focussing factor for the moon. Using Eq. 3.6 with E in units of lunar radii and v_e lunar escape velocity, one obtains a lunar focussing factor of 1.04 for the Pioneer data which compares favorably with the similar factor of 1.03 for photographic meteors (Dohnanyi, 1966).

Using these results, it follows that the flux of meteoroids into the lunar surface can be written as

$$\begin{aligned} f(m)\,dm &= Am^{-\alpha}dm, && m \geq 10^{-10}\ \text{Kg} \qquad (3.11)\\ &= A\,(10^{-10})^{\beta-\alpha}\,m^{-\beta}dm, && 5\times10^{-15}\ \text{Kg} \leq m \leq 10^{-10}\ \text{Kg}\\ &= 0 && m \leq 5 \times 10^{-15}\ \text{Kg} \end{aligned}$$

where

$$A = 1.6 \times 10^{-18}(\text{Kg})^{\alpha-1},\quad \alpha = 13/6,\quad \beta = 3/2$$

where f(m)dm is in the same units as Eq. 3.1.

The cumulative lunar flux N(m) of particles with masses of m Kg or greater, is then

$$N(m) = \int_{m}^{\infty} f(m)\,dm, \qquad (3.12)$$

with f(m) given by Eq. 3.11. The primary lunar flux Eq. 3.12 is plotted in Figure 2 together with other quantities to be discussed below.

We now proceed to estimate the flux of lunar secondaries. In order to do so, we have to estimate the mass distribution of secondary particles produced during each primary impact and then sum the respective contributions of the primary flux in any given mass range.

Following Dohnanyi (1969) we shall use the following comminution law for secondaries:

$$n(m)\,dm = (2-\eta) M_e M_b^{\eta-2} m^{-\eta} dm \qquad (3.13)$$

where $n(m)\,dm$ is the number of secondary particles produced in the mass range m to m+dm by a primary particle impacting the lunar surface. M_e is the total mass of fragments ejected from the impact crater, M_b is the upper limit on the mass of the largest fragment and η is a constant. Eq. 3.13 is based on results of experiments by Gault et al. (1963). Using numerical values from these experiments we take (cf Dohnanyi, 1969)

$$\eta = 1.8, \qquad (3.14)$$

$$M_b = .1 M_e, \qquad (3.15)$$

$$M_e = 200\ m_p \qquad (3.16)$$

where m_p is the mass of the primary projectile; using the results of Pioneer measurements, an average impact velocity of 20 km/sec has been assumed in Eq. 3.15 and 3.16.

We can now define the secondary flux $h(m)\,dm$ per square meter per sec per 2π sterad in the mass range dm as

$$h(m)\,dm = dm\ (2-\eta) \int M_e(m_p)\ [M_b(m_p)]^{\eta-2} m^{-\eta} f(m_p)\ dm_p \qquad (3.17)$$

Using numerical values from Eq. 3.14, 3.15 and 3.16, we have

$$h(m)\,dm = 139\ m^{-1.8} dm \int_{m/200}^{\infty} m_p^{.8}\ f(m_p)\,dm_p \qquad (3.18)$$

where the lower limit on the integral is the mass of the smallest primary particle which will just create a secondary with mass m as the largest fragment.

Since meteoroid sensors measure cumulative fluxes and not the differential quantities $f(m)\,dm$ and $h(m)\,dm$ (Eq. 3.11 and 3.18, respectively) we calculate and graphically display the cumulative fluxes, Eq. 3.12 and

$$H(m) = \int_m^{\infty} h(M)\,dM. \qquad (3.19)$$

The results are displayed in Figure 2, details of the calculation are given in Appendix A. The uppermost curve

in the figure is the cumulative flux H(m, sporadic) per meter^2 per second per sterad of secondary particles having a mass of m kg or greater produced by the impact into the lunar surface of the sporadic meteoroid flux F(m), in similar units. The curve labelled H(m, shower) is the contribution of meteor showers to the flux of secondaries and will be discussed below.

It can be seen that, for masses greater than 2×10^{-8}Kg, H(m, sporadic) has a slope equal to the slope of the primary flux, while for masses smaller than 2×10^{-8}Kg the slope of the secondaries equals that of the crushing law Eq. 3.13. This happens because for the larger masses the primary flux is so rich in small particles that the flux of secondaries will be proportional to the flux of the primaries. For sufficiently small masses, however, the primary flux is relatively poor in small particles and ejecta are mainly produced by relatively large particles with masses greater than 2×10^{-8}Kg.

The specific contribution of meteoroid showers to the flux of primary particles is modelled here as a multiple of the sporadic flux, Eq. 3.11, with a cutoff at a mass of 10^{-5}Kg, corresponding roughly to a fifth magnitude meteor. There is sufficient evidence (cf Dohnanyi, 1970, for theory and for references) to assume that known major showers do not contribute significantly to the flux of primary particles smaller than about 10^{-5}Kg. While no meteor showers have been reliably shown to significantly contribute to the primary flux of particles smaller than about 10^{-5}Kg, many showers have an apparent cutoff at masses substantially higher than 10^{-5}Kg

Thus we write

$$N(m, \text{shower}) = K \times N(m), \quad m \geq 10^{-5}\text{Kg}$$

$$N(m, \text{shower}) = K \times N\,(10^{-5}\text{Kg}), \quad m \leq 10^{-5}\text{Kg}$$

where K is a function, approximated here as a constant. Values for K for several well known showers have been compiled elsewhere (NASA-SP-8013) and are displayed in Figures 3 and 4. It can be seen, from these figures, that typical values for K range from 0 to about 10.

The curve, marked H(m, shower) in Figure 2, is the contribution of a meteor shower with K=1, i.e., H(m, shower) is the contribution to the secondary flux from the sporadic primary flux when the latter is cut off at 10^{-5}Kg. The

contribution of any shower is the product of H(m, shower) by the appropraite K value obtained from Fig. 3 and 4. It can readily be seen that none of the well known showers are likely to contribute significantly to the secondary flux of particles having masses much less than about 10^{-5}Kg.

It must be emphasized that A film, B film and time of flight detection is only possible for particles that have a high enough speed to produce impact ionization; in this case, calibrations (Berg, private communication) indicate a threshold velocity of about 1.5 Km/sec. Gault et al's data indicate that during impact into a semi-infinite target the fraction of the total ejected mass that acquires a velocity greater than 1.5 Km/sec, is about 4×10^{-3}. It therefore follows that of the secondary particle flux only .4% will likely be detected by the impact ionization sensors. Low velocity particles may however, still be detected by the microphones provided that they have a sufficiently large momentum.

4. Directional Effects

In this section we shall consider what effect the orientation of the detector surfaces is likely to have on the counting rate. If, e.g., most of the ejecta are ejected approximately vertically, then they will also fall down approximately vertically; in this case it is easy to see that a horizontal detecting surface will detect many more particles in a given time than would a vertical detecting surface.

We now consider the trajectory of typical ejected particles. If the ejection velocity is lower than lunar escape velocity, and if the vector velocity forms an angle θ with the vertical, then the particle will rise, reach a maximum height on its ballistic trajectory and finally fall back to the surface. Because of symmetry, the particle will impact the surface with a velocity equal in magnitude to the ejection velocity and forming an angle θ with the vertical. Also, because of this symmetry of ballistic trajectories, the time of flight during which a particle is rising equals the time of descent and hence, for a steady state secondary flux the number of "rising" particles equals the number of "descending" particles. Furthermore any vertical test surface with sufficiently large exposure and not preferentially shielded by rocks, mounds, etc. will be impacted by a number of rising particles equal to that of descending particles.

The major differences in the properties of rising particles compared with the descending ones are that (1) the descending particles always have a velocity less than lunar escape velcity while some of the ascending particles may be travelling in hyperbolic escape trajectories; (2) the descending particles arrive, on the average, from a much longer range than the ascending

particles and therefore, for a given differential solid angle of particle trajectories intercepted by the sensor, the descending particles represent a minute fraction of ejecta from a large number of remote primary events while the ascending particles comprise a significant fraction of ejecta originating from a small number of nearby primary events.

We now discuss the flux into an arbitrarily oriented test surface. Assume that during the impact of a primary particle, all secondary particles are ejected into ballistic trajectories initially forming an angle θ_o with the vertical; also assume this delta-function distribution in θ_o to be axially symmetric. It is then shown in Appendix B that the secondary flux into an arbitrary test surface whose normal forms an angle ψ with the vertical is, relative to the flux into a horizontal test surface,

$$\chi(\theta_o,\psi) = \chi^{down}(\theta_o,\psi) = \cos\psi, \qquad \theta_o \leq \pi/2-\psi \tag{4.1}$$

where $\chi(\theta_o,\psi)$ is the ratio of the flux of secondaries into the unit surface at angle ψ to the flux into a similar surface at angle $\psi = 0$. The superscript "down" means the flux of particles descending in their orbits. Since $\pi/2-\psi$ is the angle formed by the test surface with the vertical, the surface is clearly inaccessible to upgoing particles (i.e. particles rising in their orbits) for ejection angles θ_o smaller than $\pi/2-\psi$ and the entire flux into the test surface will be caused by secondary particles descending in their orbits.

For

$$\pi/2-\psi \leq \theta_o \leq \pi/2 \tag{4.2}$$

we have, from Appendix B,

$$\chi^{down}(\theta_o,\psi)=(1/\pi)\sin\psi\tan\theta_o\sin[\cos^{-1}(\cot\psi/\tan\theta_o)]+ [1-(1/\pi)\cos^{-1}(\cot\psi/\tan\theta_o)]\cos\psi \tag{4.3}$$

and

$$\chi^{up}(\theta_o,\psi)=(1/\pi)\{\sin\psi\tan\theta_o\sin[\cos^{-1}(\cot\psi/\tan\theta_o)]+ \cos\psi\cos^{-1}(\cot\psi/\tan\theta_o)\}\,. \tag{4.4}$$

Some of the properties of Eq. 4.1, 4.3 and 4.5 can be seen from Fig. 5, 6 and 7. Figure 5 is a plot of $\chi^{down}(\theta_o,\psi)$ given by Eq. 4.1 and 4.3. It can be seen from the figure,

that for large θ_o, i.e. for particles ejected almost horizontally a tilted surface or vertical surface (i.e., large ψ) will intercept more descending particles than would a horizontal test surface. This "advantage" is, however, lost when the ejection angle θ_o is about 70°; in this case the impact rate by descending particles is more or less the same regardless of the angle of tilt, ψ. For smaller θ_o, tilted surfaces will intercept a smaller particle flux than would a horizontal surface. It is quite clear that for most angles of ejection the horizontal test surface is a significantly better detector of descending particles than is a tilted surface.

Figure 6 is a plot of $\chi^{up}(\theta_o,\psi)$ given by Eq. 4.4. Since a horizontal surface cannot detect particles travelling upward, it is a very poor detector of rising particles. As one would expect, large ejection angles θ_o will improve the impact rate into the test surface for adequate tilt angles ψ. For ejection angle $\theta_o = 80°$, and tilt angle $\psi \sim 15°$, the contribution of the upgoing particles is considerable: the impact rate due to these particles is about 3 times the total rate on a horizontal surface. When $\theta_o \lesssim 60°$, the contribution of the upgoing particles to the impact rate $\chi^{up}(\theta_o,\psi)$ decreases with decreasing θ_o.

Figure 7 is the total impact ratio $\chi^{up}(\theta_o,\psi) + \chi^{down}(\theta_o,\chi)$. It is readily seen that for large θ_o this impact rate is much greater for a tilted surface than for a horizontal one. For ejection angles of about 50° or smaller, the impact rate is lower for all tilted surfaces compared with the horizontal surface. We may, therefore, conclude that the horizontal surface of the lunar experiment will be a more efficient detector of ejecta with small θ_o and the vertical surfaces will be more efficient in detecting ejecta with large values of θ_o.

A word of caution is, however, in order: the contribution of the upgoing ejecta is not likely to manifest itself as a steady flux. For $\theta_o = 45°$, for example, all particles that contribute to the ascending flux, F^{up}, will originate in impacts at an approximate distance from the detector, equal to its height h above the ground. On the other hand, on the assumption of a flat moon, the descending flux, F^{down}, will consist of ejecta produced at a distance $D = v^2 \sin 2\theta/g$, where v is the speed of the ejecta and g is the lunar gravitational acceleration. For $v = 1.5$ km/sec and $\theta_o = 45°$ this gives $D = 1.4 \times 10^3$ km. It therefore follows that F^{down} will be a more

or less steady flux of a fixed number of particles hitting the detector in unit time, but F^{up} will consist of sporadic "bursts". Each such burst will contain many ejected particles from nearby, and the rate of these bursts is likely to be about $(h \cot \theta_o)/v^2 \sin 2\theta_o/g)$ smaller than the impact rate of the down-coming particles. For $\theta_o = 45°$ and h = 1 meter this factor is about 10^{-6}, and is readily seen that for limited periods of exposure, one is very unlikely to encounter up-going ejecta. We shall therefore prefer to use Figure 5, rather than Figure 7, for estimating the impact rates to be expected.

In order to estimate the nominal counting rate on the lunar surface, we consider Figure 8. This is a plot of ejection velocity v vs ejection angle θ_o for secondaries produced in the laboratory (Gault et al., 1963). It can be seen, that for particles faster than about 1.5 km/sec, $\theta_o \gtrsim 40°$. Since the number of secondaries decreases rapidly with increasing ejection speed, it may be assumed that most of the secondaries that will be detected correspond to an ejection angle of about 40° or 50°. Returning now to Figure 5, we see that $\theta_o \sim 40°$ or 50° reduces the counting on the vertical surfaces to about 30% or 40% of the counting rate for a horizontal detecting surface.

5. Discussion and Results

Using the information developed in the previous sections, one can calculate the expected number of impacts that the instrument will detect. The result is summarized in Table 1, where the detectable daily impact rates by primary and secondary particles are listed for each sensor, as indicated. For the ejecta, an average speed of 100 m/sec has been employed (cf Zook, 1967) and an ejection angle of $\theta = 45°$. Such a choice for θ is in agreement with empirical results by Gault et al., (1963). It should be pointed out that the impact rates of ejecta rising in their trajectories are underestimated inasmuch as particles with a velocity exceeding lunar escape have not been included in the calculation. Because of the rapid decrease of the number of ejecta with ejection speed, such fast particles are not expected to contribute substantially to the impact rate. Furthermore, the measured impact rates of ascending particles are not the true impact rates, but represent large numbers of simultaneous impacts on the detector that originate in nearby meteoroid impacts on the lunar surface separated by long time intervals. Individual impacts cannot be resolved when such bursts occur.

It is readily seen from Table 1 that secondary events will outnumber primary events by a factor of about 10 to 20 for all sensors except the microphones, which will count about

10^2 times more secondaries than primaries. We, expect therefore, that detection and identification of primary meteoroids will only be possible with the TOF sensor because the latter measures particles velocity vector as well as kinetic energy.

Using the principle of energy conservation, Boyle and Orrok (1963) have shown that the integrated flux of kinetic energy of secondaries cannot exceed that of the primaries. Since the TOF and A and B film detection is only possible for particles having a kinetic energy in excess of a threshold value, it may appear surprising that we estimate a much higher detection rate for secondaries than for primaries (Table 1). It can readily be shown, however, that the integrated kinetic energy fluxes, defined by the present model do not violate Boyle and Orrok (1963) but are sensitive to the assumed cut-off in the primary flux at 5×10^{-15}Kg and the "flattening" of the slope, on a doubly logarithmic plot, of the primary flux for particles smaller than 10^{-10}Kg.

Table 1 indicates that the expected counting rates will vary considerably from sensor to sensor. Microphones are expected to register several secondary impacts a day, while the TOF measurement rate for primaries is expected to be only about one event every four months for the East looking sensor. The absolute counting rates as well as the relative counting rates of each sensor are sensitive functions of the model environment, e.g. an angular distribution of ejecta which is significantly different from our simple model, will give rise to different relative counting rates for the sensors. If the comminution law for cratering in lunar material is appreciably different from the present model, the absolute counting rates of the LEAM sensors would correspondingly depart from the estimates of Table 1. Consequently, the counting rates of the LEAM detectors will indicate a micrometeoroid environment that can be defined and interpreted with the use of the present analysis.

6. Acknowledgments

Thanks are due to O. E. Berg and U. Gerloff for their communications of unpublished data and for many helpful discussions.

2015-JSD-bab

J. S. Dohnanyi

Attachments
Appendixes A&B
Table 1
Figures 1-8
B1 & 2

REFERENCES

Berg, O. E. and F. F. Richardson, The Pioneer 8 Cosmic dust experiment, Rev. Sci. Inst. 40, 1333-1337, 1969.

Berg, O. E. and U. Gerloff, Orbital Elements of Micrometeoroids Derived from Pioneer 8 Measurements, J. Geophys. Res. 75, 6932-6939, 1970, a.

Berg. O. E. and U. Gerloff, More than two years of micrometeorite data from two Pioneer Satellites, XIIIth Planery Meeting, COSPAR, Leningrad, 1970, b.

Boyle, W. S. and G. T. Orrok, Penetration of Spacecraft by Lunar Secondary Meteoroids, AIAA Journal, 1, 2402-2404, 1963.

Dohnanyi, J. S. Model Distribution of Photographic Meteors, Bellcomm Technical Report, TR-66-340-1, 1966.

Dohnanyi, J. S. Collisional Model of Asteroids and Their Debris, J. Geophys. Res. 74, 2531-2554, 1969.

Dohnanyi, J. S. On the Origin and Distribution of Meteoroids, J. Geophys. Res. 75, 3468-3493, 1970.

Gault, D. E., E. M. Shoemaker and H. J. Moore, Spray Ejected from the Lunar Surface by Meteoroid Impact, NASA TND-1767, 1963.

Gerloff, U. and O. E. Berg, A Model for Predicting the Results of "in situ" Meteoroid Experiments, XIIIth Planery Meeting, COSPAR, Leningrad, 1970.

Opik, E. J. Collision Probabilities with the Planets and the Distribution of Interplanetary Matter, Proc. Royal Irish Acad. 54, 165-199, 1951.

Zook, H. A. The Problem of Secondary Ejecta Near the Lunar Surface, National Symposium of American Astronautical Society, Huntsville, Ala., 1967.

APPENDIX A

This Appendix gives an explicit formula for the cumulative flux of ejecta H(m) (Eq. 3.18)

$$H(m) = \int_m^\infty h(M)\,dM \,. \qquad \text{(A-1)}$$

This means that we merely have to perform the indicated quadrature. Using the definition of h(m)dm (eq. 3.18) we have

$$h(m)\,dm = 139\ m^{-1.8}dm \int_{m/200}^{\infty} m_p^{.8}\ f(m_p)\,dm_p \qquad \text{(A-2)}$$

where f(m) is given by Eq. 3.11. We see that the form of h(m)dm will be different depending on

$$m \lessgtr 200\mu = 2 \times 10^{-8}\text{Kg}; \qquad \text{(A-3)}$$

The influence on h(m)dm of the cutoff on f(m) at $m = 5 \times 10^{-15}$Kg can be shown to be small and is therefore neglected.

It is then straightforward to show that

$$H(m) = 2.128 \times 10^{-6} + 7.820 \times 10^{-12}m^{-.8} - 1.404 \times 10^{-9}m^{-.5},\ m \leq 2 \times 10^{-8}\text{Kg} \qquad \text{(A-4)}$$

and

$$H(m) = 3.62 \times 10^{-15}m^{-7/6},\ m \geq 2 \times 10^{-8}\text{Kg}, \qquad \text{(A-5)}$$

which is the desired result.

APPENDIX B

In this appendix, formulas will be derived for the flux of secondary particles into a test surface oriented at an angle ψ from the horizontal for various angular distributions of ejecta produced during a given impact event.

Let us consider a plane test area of magnitude da, inclined to the xy plane at an angle ψ, and so oriented that its normal $d\vec{a}$ is in the xz plane.

$$d\vec{a} = da \sin\psi \, \hat{i} + da \cos\psi \, \hat{k} \tag{B-1}$$

where $\hat{i}$, $\hat{j}$ and $\hat{k}$ are the unit vectors in the x, y and z directions, respectively.

Now consider a vector $d\vec{l}$ of arbitrary orientation and length dl:

$$d\vec{l} = dl \sin\theta \cos\phi \hat{i} + dl \sin\theta \sin\phi \, \hat{j} + dl \cos\theta \, \hat{k} \tag{B-2}$$

as illustrated in Figure B-1.

We now calculate the volume Vol of the parallelepiped with base $d\vec{a}$ and axis $d\vec{l}$:

$$Vol = d\vec{a} \cdot d\vec{l} = dadl \, (\sin\psi \sin\theta \cos\phi + \cos\psi \cos\theta) \tag{B-3}$$

Now let $d^3 n(v,\theta,\phi)\, dvd\theta d\phi$ be the number of secondaries per unit volume having a velocity in the range v to v+dv, and direction in the range θ to $\theta+d\theta$ and ϕ to $\phi+d\phi$. Assuming symmetry with respect to ϕ, we have:

$$d^3 n(v,\theta,\phi) dvd\theta d\phi = d^2 n \, (v,\theta) dvd\theta \, \left(\frac{d\phi}{2\pi}\right). \tag{B-4}$$

If, in Eq. B-3, we let

$$dl = vdt \tag{B-5}$$

then it readily follows that Vol x $d^3 n \, dvd\theta d\phi$ is the number of secondaries impacting $d\vec{a}$ during a time dt from angular directions θ to $\theta+d\theta$ and ϕ to $\phi+d\phi$.

The flux of secondaries from the direction θ and ϕ is then

$$d^3F_\psi(v,\theta,\phi)dvd\theta d\phi = \frac{\text{Vol x } d^3n\ dvd\theta d\phi}{da\ \ dt}$$
$$= vd^2n(v,\theta)dvd\theta\ \frac{d\phi}{2\pi}\ (\sin\psi\ \sin\theta\ \cos\phi + \cos\psi\ \cos\theta) \qquad (B\text{-}6)$$

and the flux of particles with all velocities and from every direction is obtained by integrating Eq. B-6 over suitable limits.

We now introduce the simplifying assumption that all secondaries are ejected into a trajectory forming, initially, an angle θ_o with the vertical. Near the lunar surface all secondaries will then be travelling at an angle θ_o with the vertical, going up, or an an angle $\pi-\theta_o$ with the vertical going down. More precisely, we take

$$d^2n(v,\theta)dvd\theta = dn(v)dv\ [\delta(\theta-\theta_o) + \delta(\theta-[\pi-\theta_o])]d\theta\,. \qquad (B\text{-}7)$$

This angular distribution for secondaries is convenient because of its simplicity and because any arbitrary distribution can be expressed as a suitable linear combination of such delta function expressions.

Combining Eq's B-6 and B-7, and using Figure B-2 it can readily be shown that the flux of dF(v)dv integrated over all directions is:

$$dF_\psi(v)dv = \frac{v}{2\pi}\,dn(v)dv\ x$$
$$\left\{ \int_{\pi/2+\psi}^{\pi} d\theta \int_{o}^{2\pi} d\phi\,[\sin\psi\ \cos\phi\ \sin\theta + \cos\psi\ \cos\theta]\ [\delta(\theta-\theta_o) + \delta(\theta-[\pi-\theta_o)] \right.$$
$$\left. + \int_{\frac{\pi}{2}-\psi}^{\frac{\pi}{2}+\psi} d\theta \int_{-\pi+\alpha}^{\pi-\alpha} d\Phi\ [\sin\psi\ \cos\phi\ \sin\theta + \cos\psi\ \cos\theta][\delta(\theta-\theta_o) + \delta(\theta-[\pi-\theta_o])] \right\} \qquad (B\text{-}8)$$

where

$$\alpha = \cos^{-1}(\cot\psi/\tan\theta_o) . \tag{B-9}$$

The first integral in Eq. B-8 is the contribution to the flux if $\theta_o < \Pi/2 - \psi$; in this case the second integral in Eq. B-8 vanishes and so does the contribution of the upgoing flux which is completely shielded from the test surface. All impacts are caused by secondaries falling back to the lunar surface. Using Eq. B-8, we then have

$$dF_\psi(v)dv = vn(v)dv \cos\psi \cos\theta_o, \ \theta_o \leq \frac{\Pi}{2} - \psi . \tag{B-10}$$

We now consider the separate contributions of the upgoing flux dF^{up} and down coming flux dF^{down} when $\Pi/2-\psi \leq \theta_o \leq \Pi/2$. The first integral in Eq. B-8 vanishes and we have:

$$dF_\psi^{down}(v)dv = \frac{vn(v)dv}{\Pi} \{\sin\psi \sin\theta_o \sin[\cos^{-1}(\cot\psi/\tan\theta_o)]$$

$$+ [\Pi - \cos^{-1}(\cot\psi/\tan\theta_o)] \cos\psi \cos\theta_o\},$$

$$\Pi/2 - \psi \leq \theta_o \leq \Pi/2 \tag{B-11}$$

and

$$dF_\psi^{up}(v)dv = \frac{vn(v)dv}{\Pi} \{\sin\psi \sin\theta_o \sin[\cos^{-1}(\cot\psi)/\tan\theta_o]$$

$$+ \cos\psi \cos\theta_o \cos^{-1}[\cot\psi/\tan\theta_o]\}. \tag{B-12}$$

In the present study, we are interested in the magnitude of the flux at different angles ψ compared with the flux for a horizontal detector, $\psi=0$. We shall therefore calculate

$$\chi(\theta_o,\psi) = \frac{dF\psi}{dF_{\psi=0}} \tag{B-13}$$

for the various cases, Eq. B-10, 11 and 12. The result is

$$\chi(\theta_o,\psi) = \cos\psi, \ \theta_o \leq (\Pi/2) - \psi \tag{B-14}$$

$$\chi^{down}(\theta_o,\psi) = \frac{\sin\psi \tan\theta_o}{\pi} \sin[\cos^{-1}(\cot\psi/\tan\theta_o)] +$$

$$[1-\frac{1}{\pi}\cos^{-1}(\cot\psi \tan\theta_o)] \cos\psi,$$

$$\pi/2-\psi \leq \theta_o \leq \pi/2 \qquad \text{(B-15)}$$

and

$$\chi^{up}(\theta_o\psi) = \frac{1}{\pi}\{\sin\psi \tan\theta_o \sin[\cos^{-1}(\cot\psi/\tan\theta_o)] +$$

$$+ \cos\psi \cos^{-1}(\cot\psi/\tan\theta_o)]\}. \qquad \text{(B-16)}$$

The formulas for $\chi^{up}(\theta_o,\psi)$, $\chi^{down}(\theta_o,\psi)$ and their sum are plotted in Figure 5, 6 and 7 respectively.

TABLE 1

ESTIMATED IMPACT RATES ON THE LEAM DETECTORS

		Primaries	Secondary Ejecta	
			Down	Up
Horizontal Detector	A-film*	8.5×10^{-2}/day	1.4/day	0
	TOF**	1.5×10^{-2} "	.24 "	0
	4"x4" mike***	2.0×10^{-2} "	2.5 "	0
East Looking Detector	A-film*	4.2×10^{-2}/day	.42/day	> .42/day
	TOF**	7.4×10^{-3}/day	7.4×10^{-2}/day	$>7.4 \times 10^{-2}$/day
	4"x4" mike***	1×10^{-2}/day	.8/day	> .8/day
West Looking Detector	B-film*	4.3×10^{-2}/day	.12/day	> .12/day
	1"x4" mike	8.5×10^{-3}/day	.65/day	> .65/day
	3"x4" mike	2.5×10^{-2}/day	2.0/day	>2.0/day

* Using an angle of acceptance of π sterad

** Using a TOF rate of .175 x A-film detection rate.

*** Using an angle of acceptance of .98 sterad

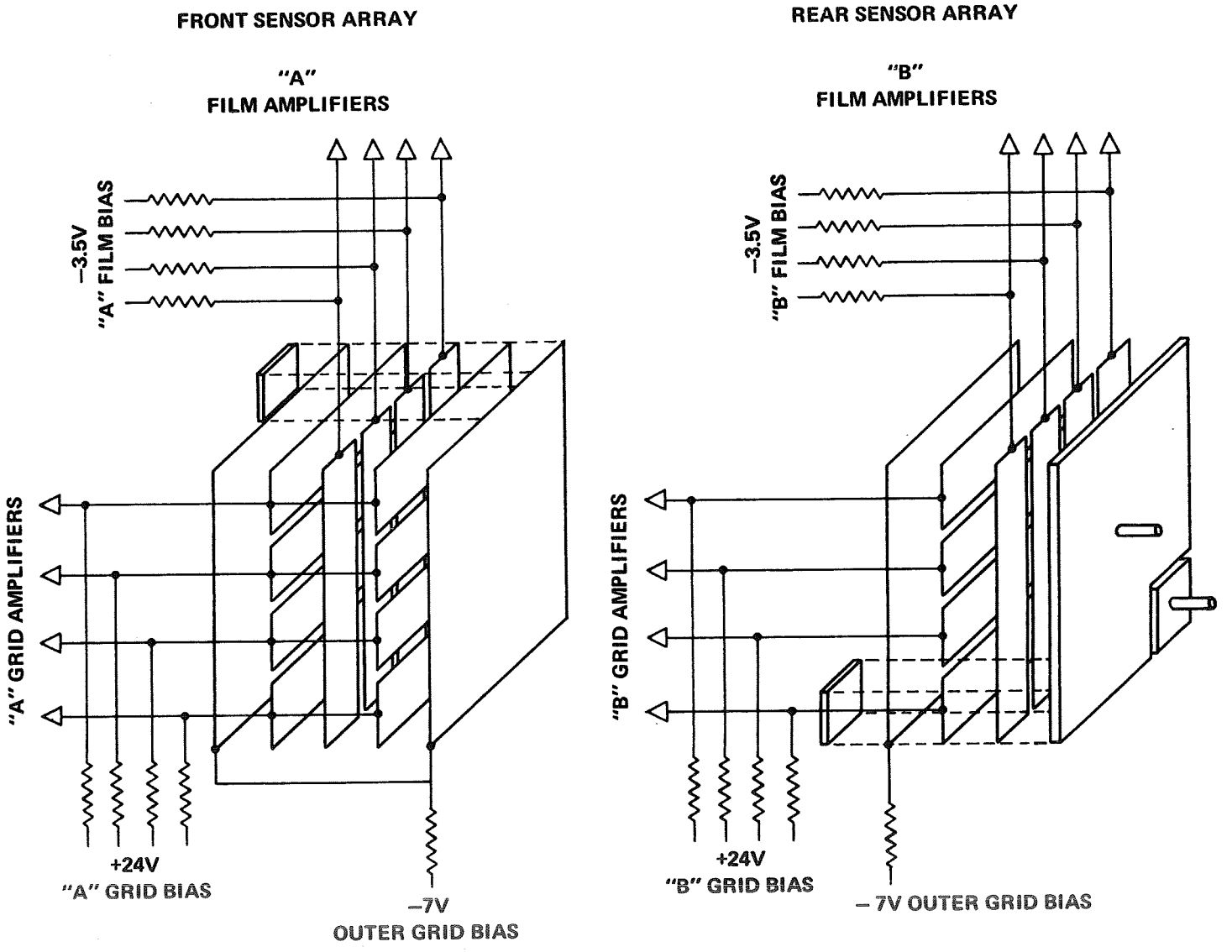

FIGURE 1 - SCHEMATIC VIEW OF THE PIONEER SENSOR

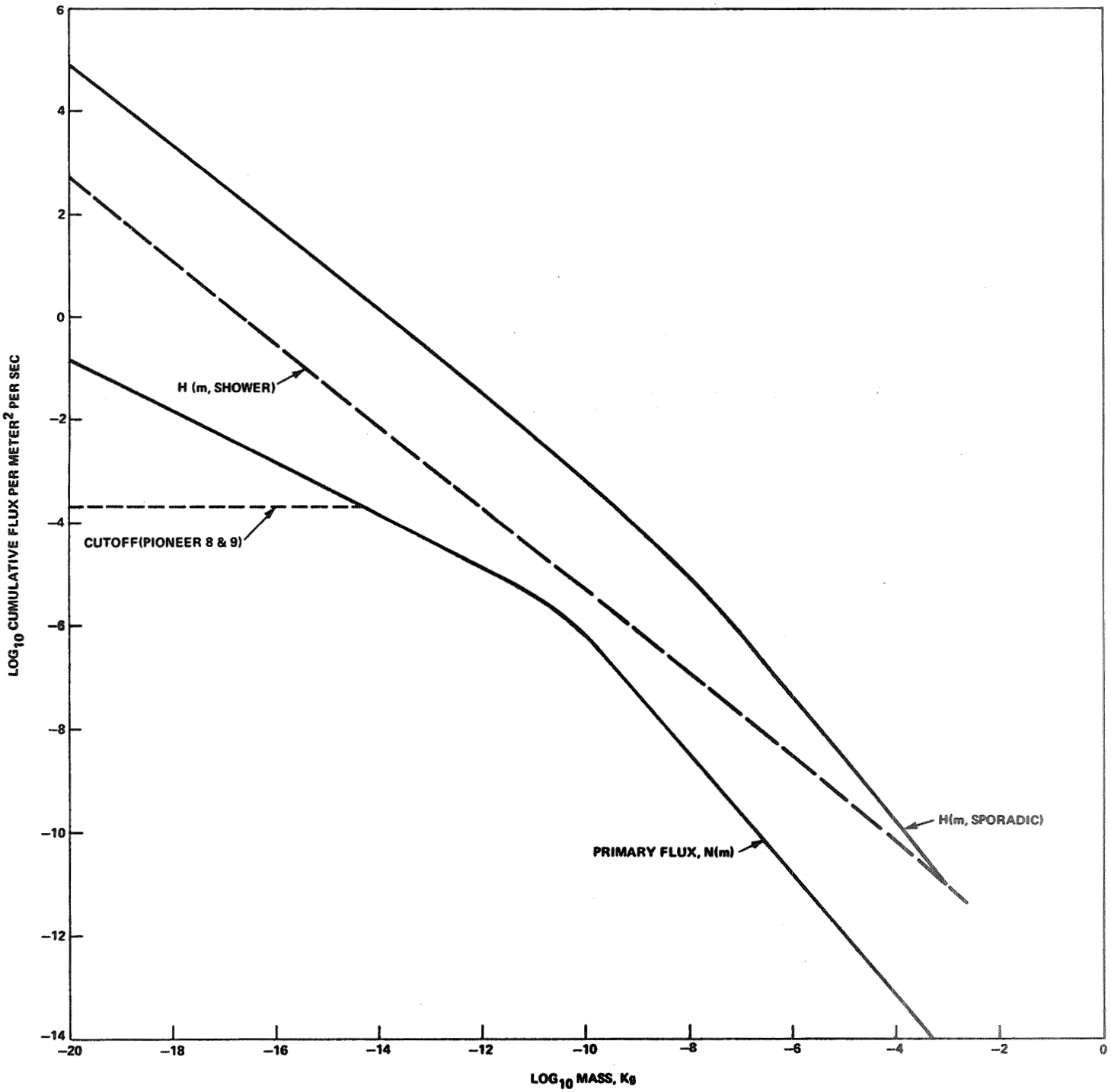

FIGURE 2 - CUMULATIVE FLUX OF PRIMARIES N(m) AND EJECTA H (m, SHOWER) PRODUCED BY SHOWER PRIMARIES

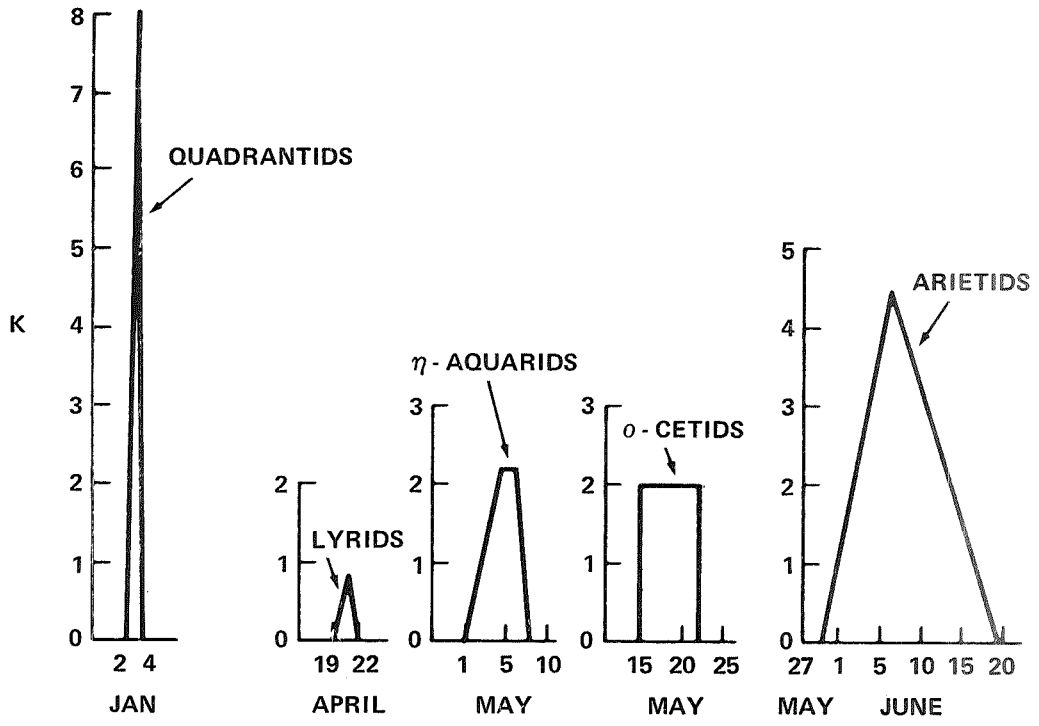

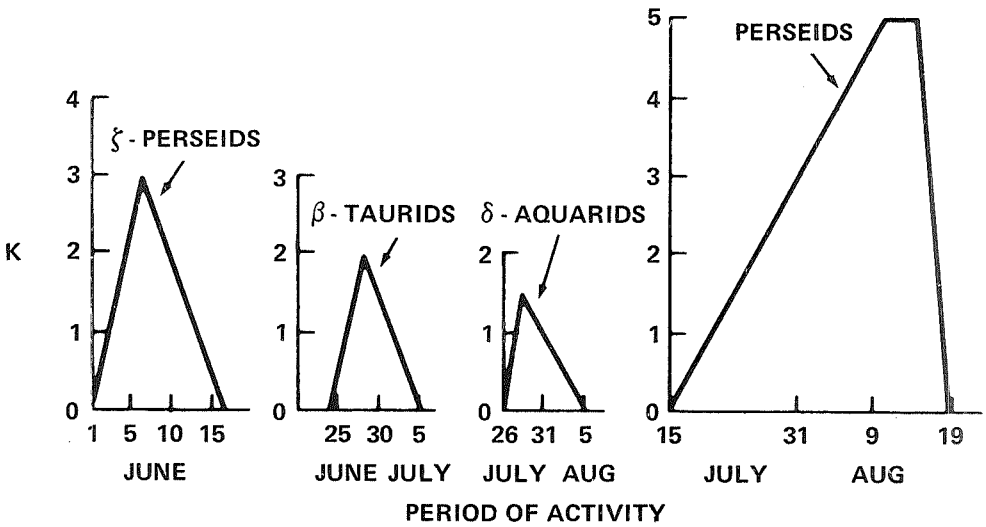

$$K = \frac{\text{CUMULATIVE FLUX OF STREAM}}{\text{AVERAGE CUMULATIVE SPORADIC FLUX}}$$

FIGURE 3 - ACTIVITY RATIO FACTOR VERSUS PERIOD OF ACTIVITY (JANUARY – AUGUST) FOR MAJOR STREAMS BASED ON PHOTOGRAPHIC METEORS WITH MASS, $m \geqslant 10^{-1}$ GRAM

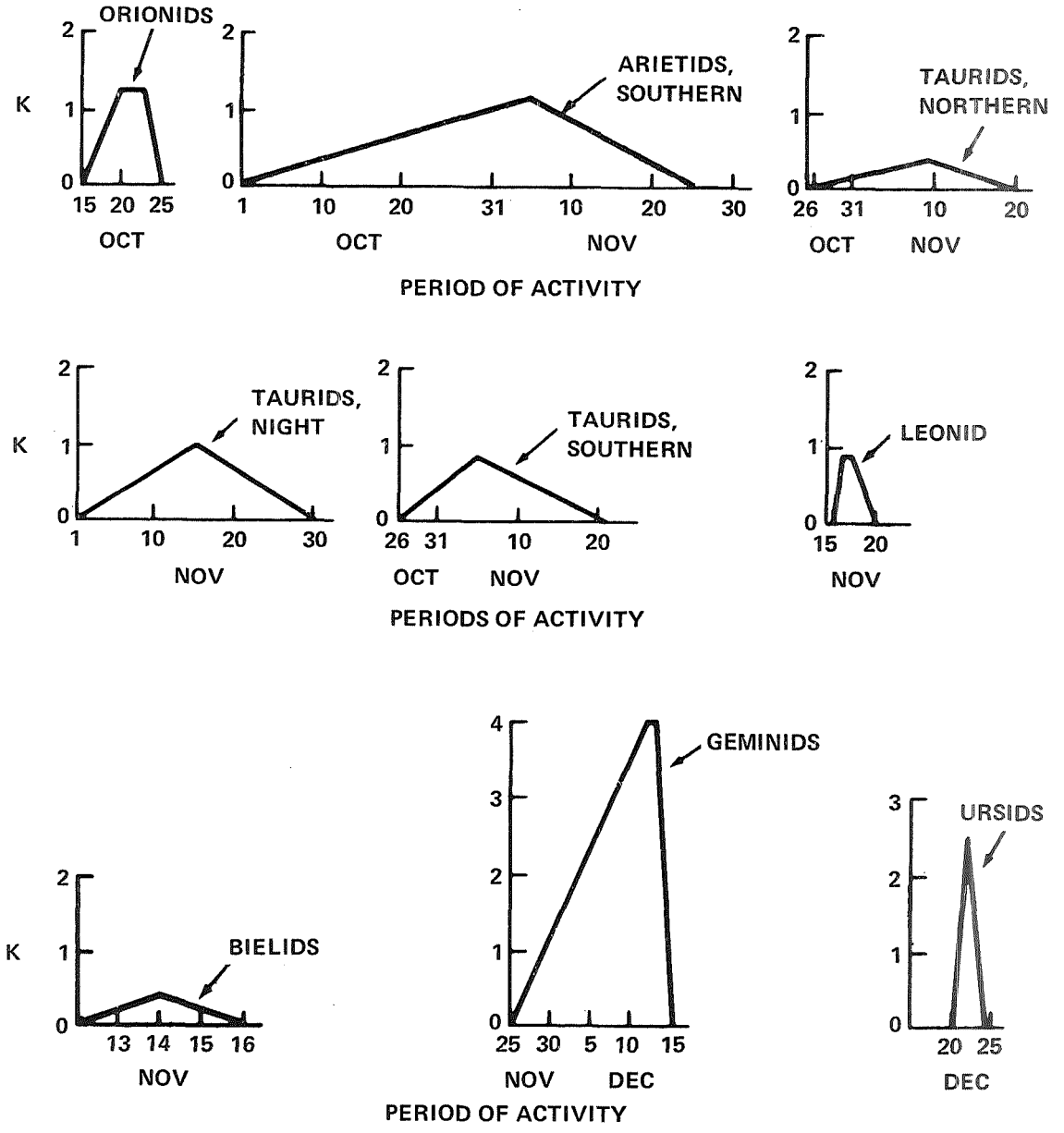

$$K = \frac{\text{CUMULATIVE FLUX OF STREAM}}{\text{AVERAGE CUMULATIVE SPORADIC FLUX}}$$

FIGURE 4 - ACTIVITY RATIO FACTOR VERSUS PERIOD OF ACTIVITY (SEPTEMBER – DECEMBER) FOR MAJOR STREAMS BASED ON PHOTOGRAPHIC METEORS WITH MASS, $m \geqslant 10^{-1}$ GRAM

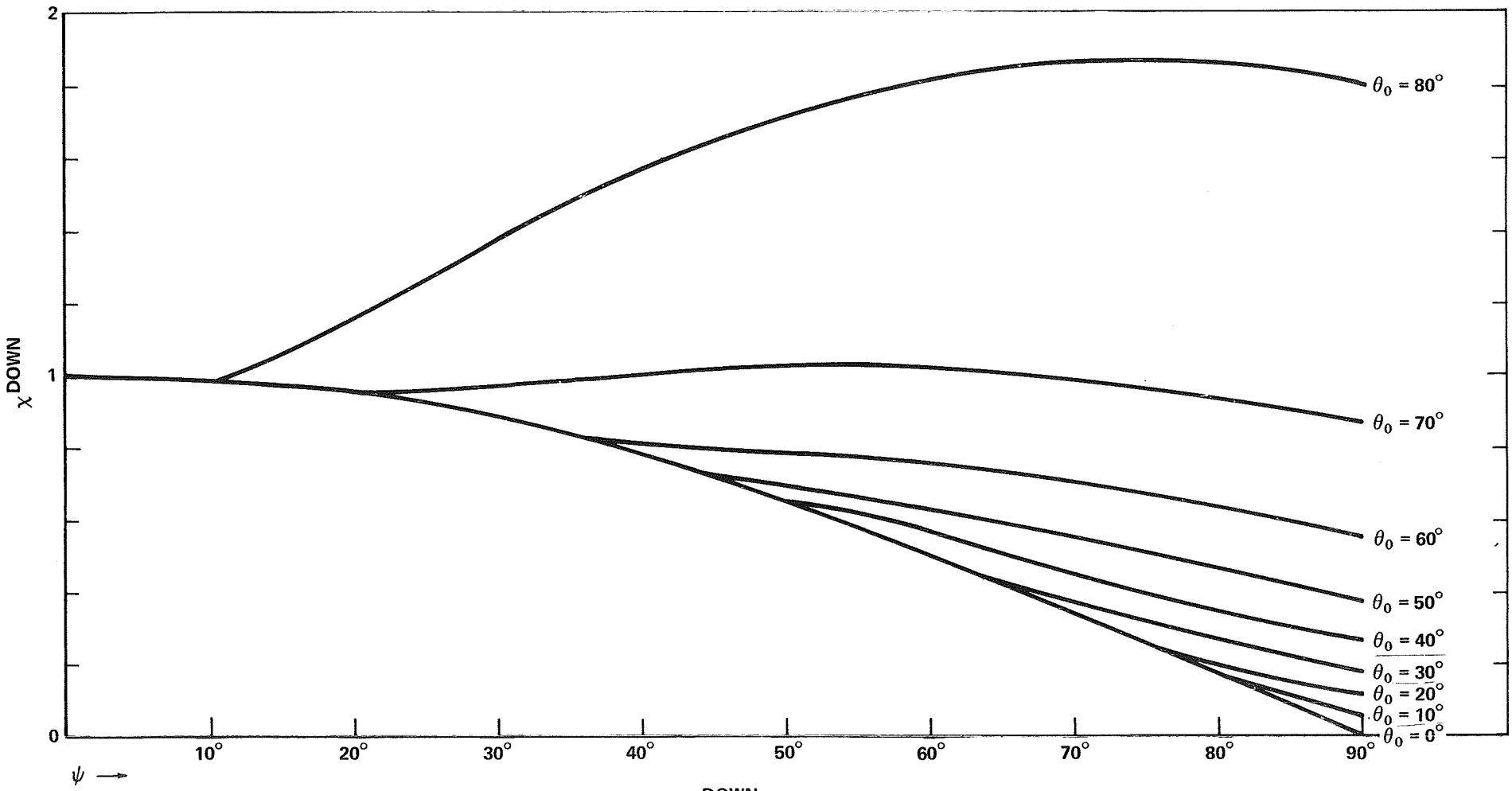

FIGURE 5 - RATIO OF THE FLUX OF PARTICLES, X^{DOWN}, DESCENDING IN THEIR BALLISTIC TRAJECTORIES INTO A SURFACE, TILTED AT ANGLE ψ WITH THE HORIZONTAL, TO THE SAME FLUX INTO A HORIZONTAL SURFACE OF THE SAME SIZE. θ_0 IS THE ANGLE FORMED BY THE INCIDENT PARTICLE TRAJECTORY WITH THE VERTICAL

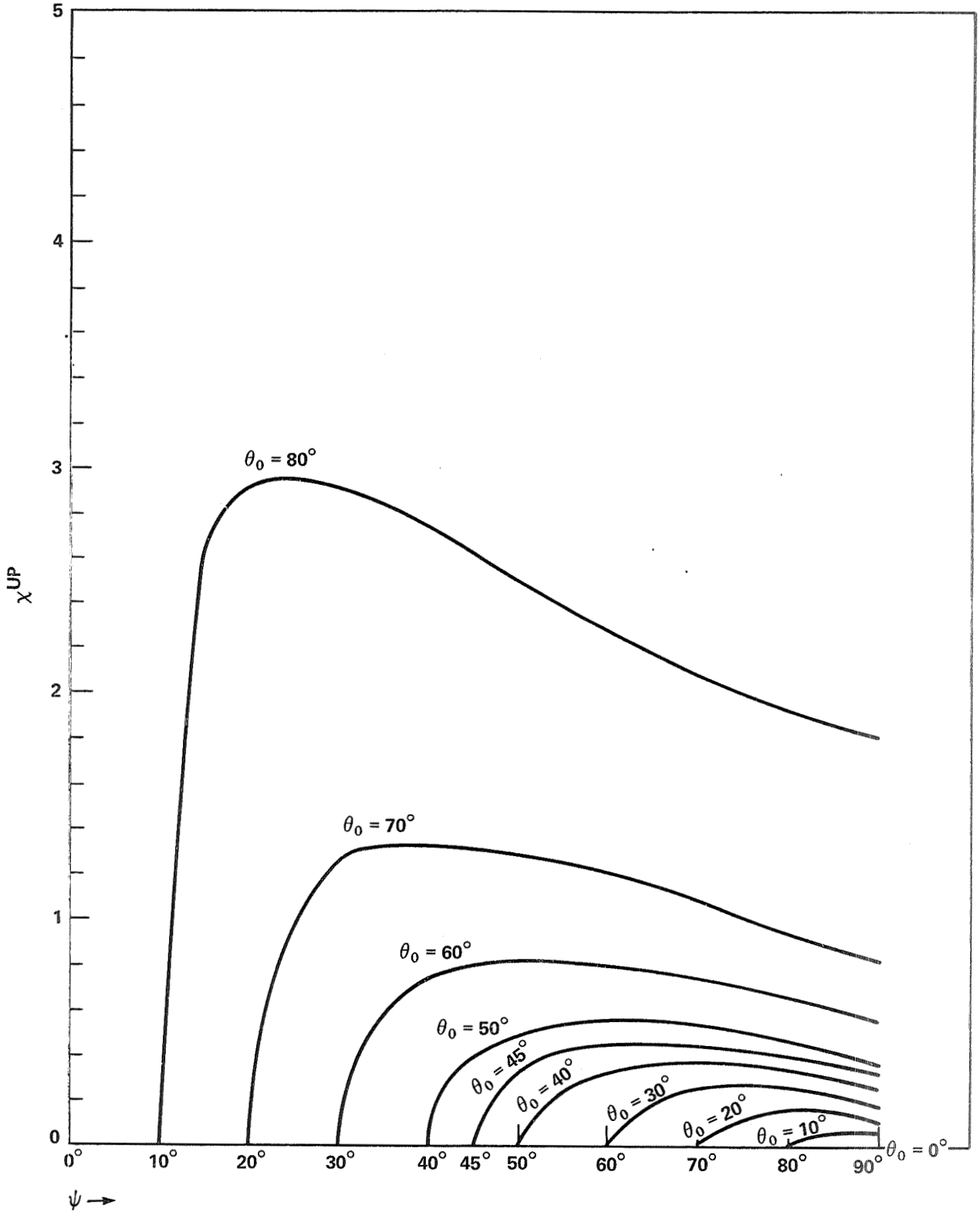

FIGURE 6 - RATIO OF THE FLUX OF PARTICLES, X^{UP} RISING IN THEIR BALLISTIC TRAJECTORIES INTO A SURFACE, TILTED AT ANGLE ψ WITH THE HORIZONTAL, TO THE FLUX OF (DESCENDING) PARTICLES INTO A HORIZONTAL SURFACE OF THE SAME SIZE

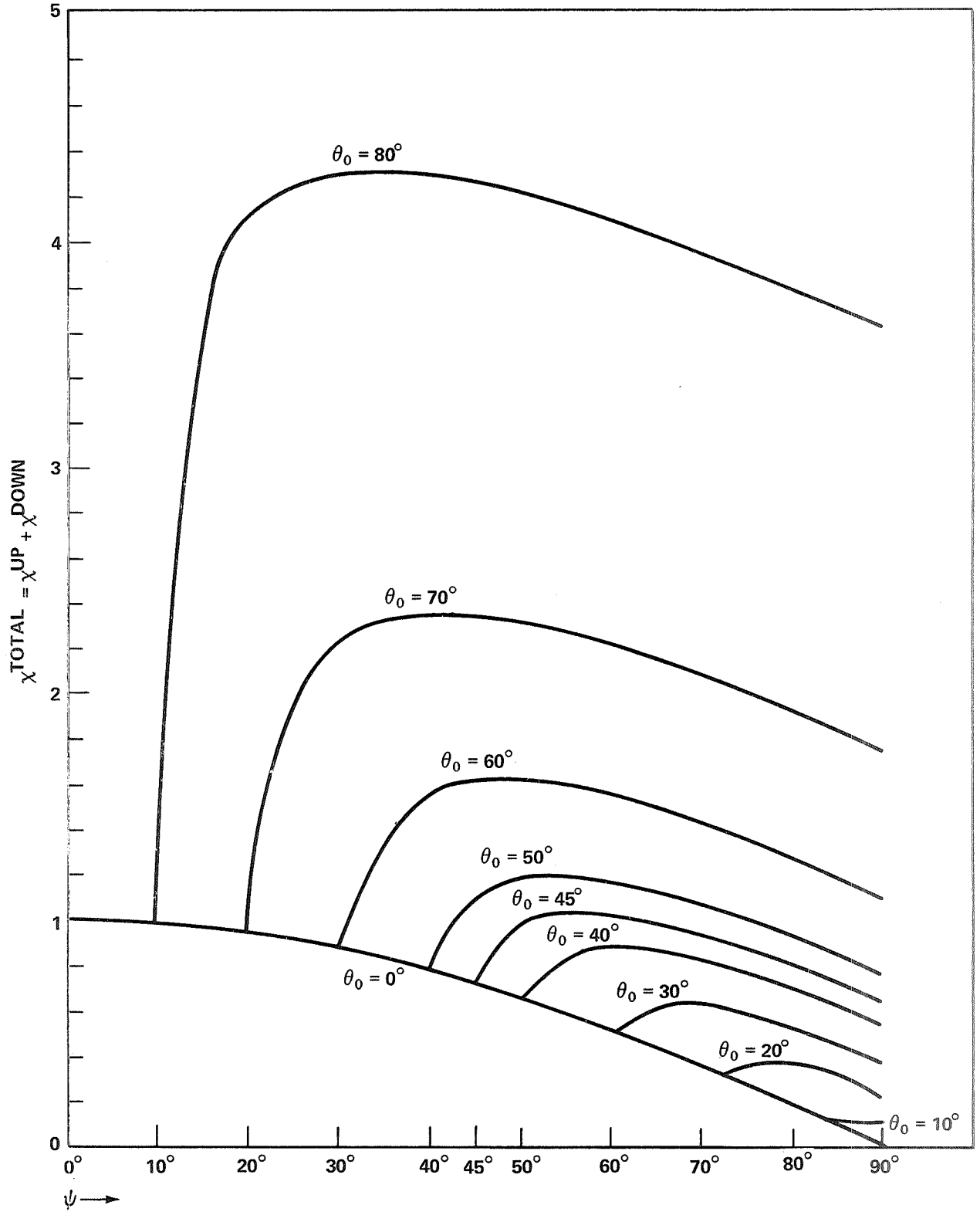

FIGURE 7 - RATIO OF THE TOTAL FLUX OF PARTICLES, $X^{UP} + X^{DOWN}$, INTO A TEST SURFACE, TILTED AT ANGLE ψ WITH THE HORIZONTAL, TO THE FLUX OF (DESCENDING) PARTICLES INTO A HORIZONTAL SURFACE OF THE SAME SIZE

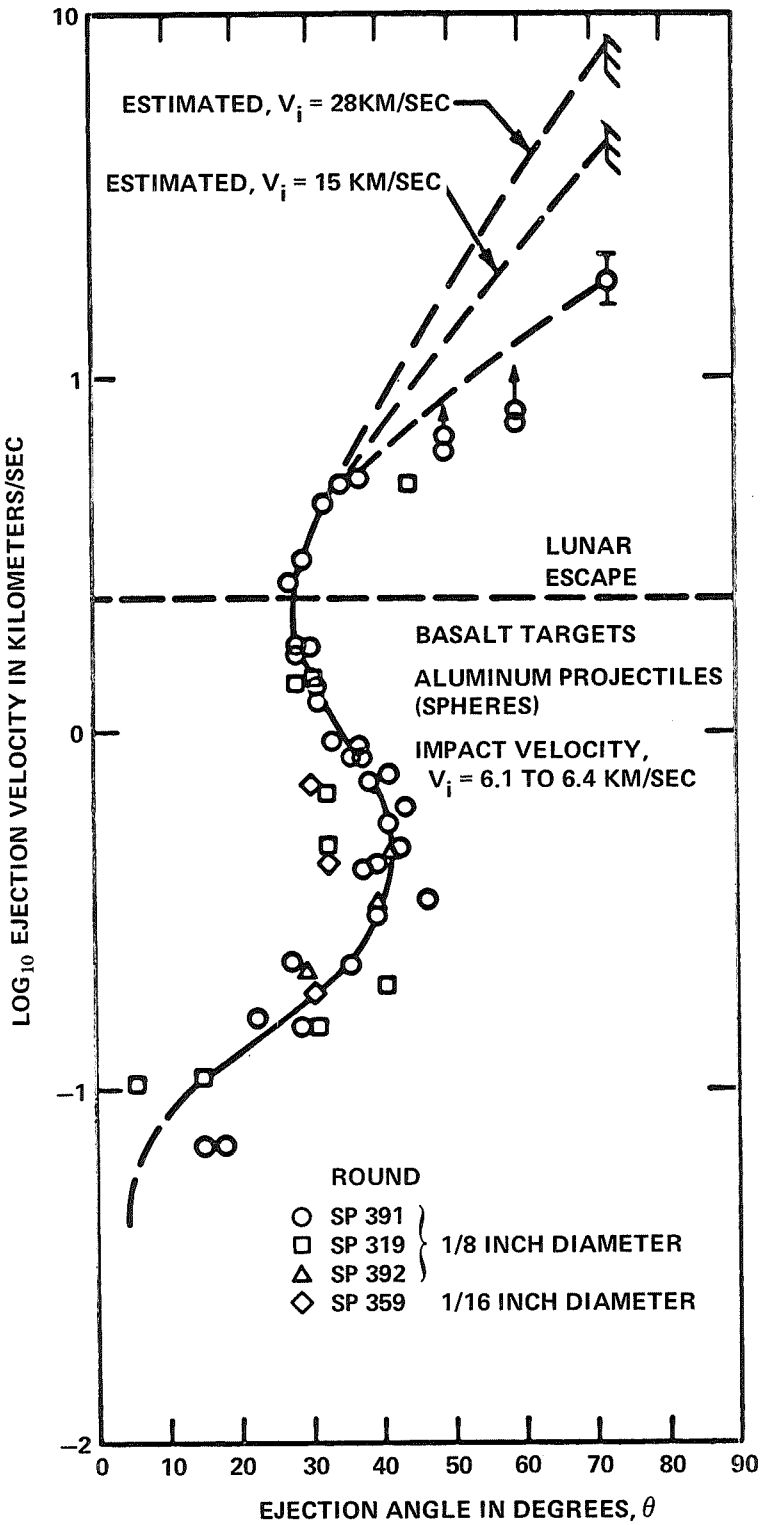

FIGURE 8 - VARIATION OF EJECTION VELOCITY WITH EJECTION ANGLE FOR FRAGMENTS THROWN OUT OF CRATERS FORMED IN BASALT BY HYPERVELOCITY IMPACT

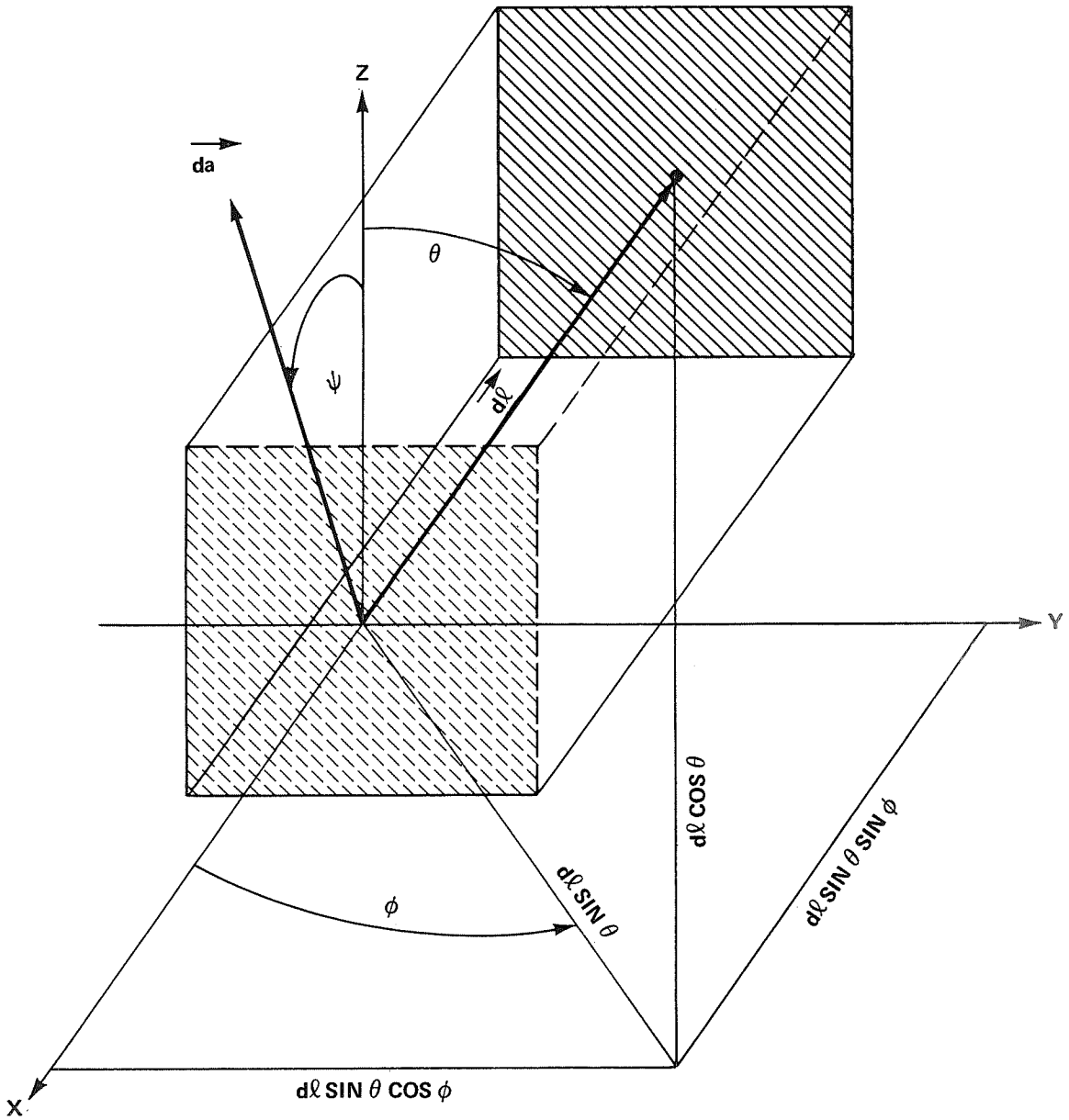

FIGURE B-1 - GEOMETRICAL ILLUSTRATION FOR DERIVING EQUATION B-6 IN THE TEXT

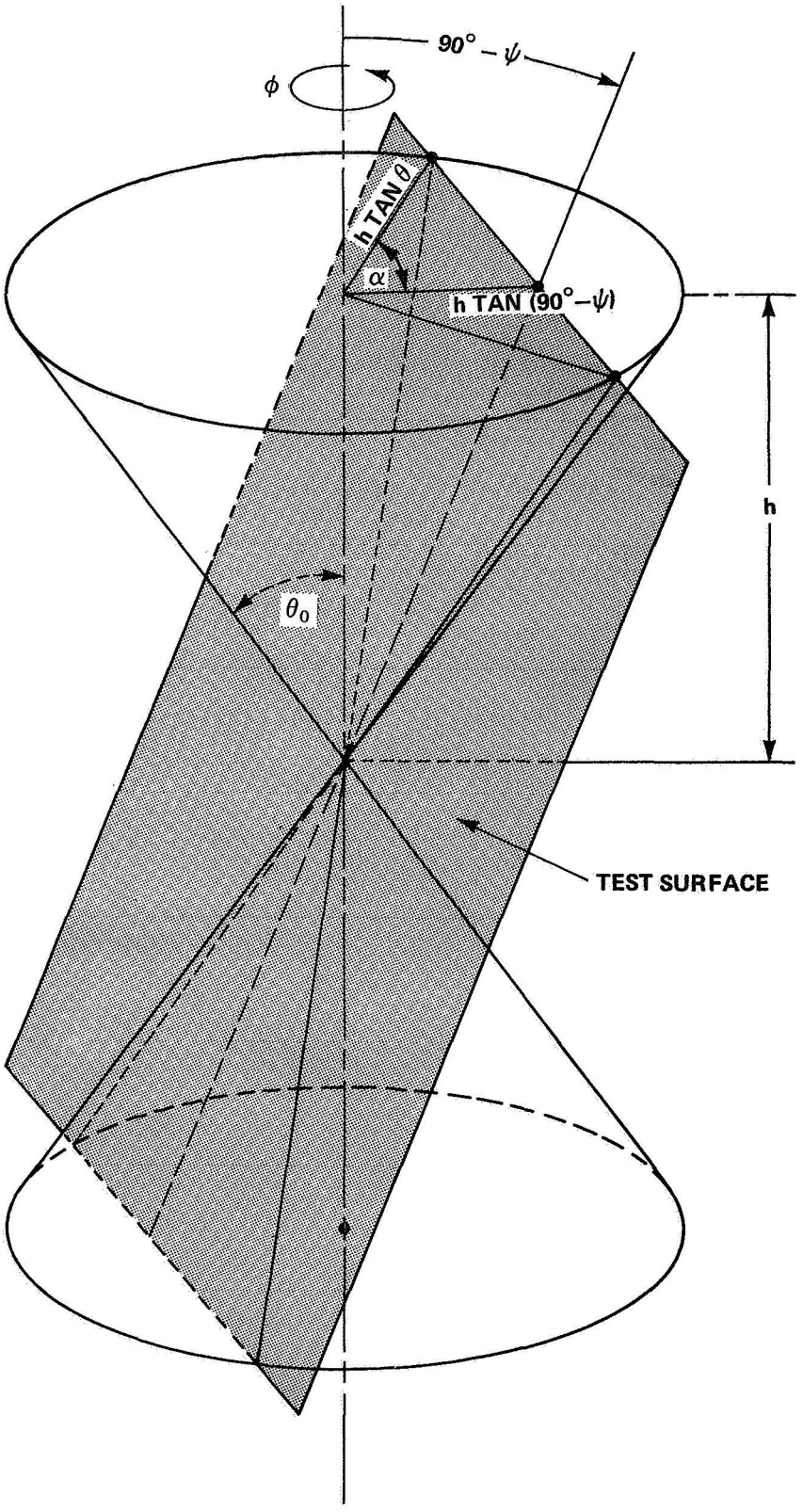

FIGURE B-2 - GEOMETRIC CONSTRUCTION DEFINING THE LIMITS OF INTEGRATION FOR EQUATION B-8 IN THE TEXT FOR EJECTA WITH ANGULAR DISTRIBUTION $\theta_0 \geqslant 90^\circ - \psi$, IT IS READILY SEEN THAT COS α = TAN $(90^\circ - \psi)$/TAN θ